

Isogeometric Analysis on Trimmed Solids: A B-Spline-Based Approach Focusing on Explicit Dynamics

Manuel Meßmer¹, Lukas Leidinger², Stefan Hartmann², Frank Bauer³, Fabian Duddeck⁴, Roland Wüchner¹, Kai-Uwe Bletzinger¹

¹Technical University of Munich, Chair of Structural Analysis
Arcisstr. 21, D-80333 München, Germany
e-mail: manuel.messmer@tum.de, web page: www.st.bgu.tum.de

²DYNAmore GmbH, Industriestr. 2, D-70565 Stuttgart, Germany

³BMW Group, Knorrstr. 147, D-80788 Munich, Germany

⁴Technical University of Munich, Associate Professorship of Computational Mechanics,
Arcisstr. 21, D-80333 München, Germany

1 Introduction

Engineering workflows are habitually split into a modelling phase and a consecutive analysis phase, which is primarily driven by the finite element method (FEM). However, bridging the gap between design and analysis remains a sophisticated problem and may consume a vast amount of computational as well as manual operations, especially in highly iterative development processes. To avoid this major bottleneck, Isogeometric Analysis (IGA) [1] and later Isogeometric B-Rep Analysis [2] were developed. They rely on the mathematical descriptions of Computer Aided Design (CAD), such as NURBS- and B-Spline-based boundary representation (B-Rep) models. However, classical B-Rep formulations describe a solid only by its boundary faces and do neither provide any physical nor geometrical description of the interior. Therefore, the IGA concept cannot be applied to three-dimensional structures in a straightforward manner.

To overcome this issue and to facilitate the modelling with solid-based formulations, a design-through-analysis workflow is presented which avoids demanding boundary-fitted meshes. The focus lies on a fully automated CAD-integrated analysis for 3D solid models in the scope of explicit dynamics and crash simulations. Therefore, efficiency with respect to time step size and cost per time step plays a key role in our approach and distinguishes it from already existing methods. In a first step, the geometry is retrieved from the CAD system as a stereolithography (STL) representation and embedded into the parameter space of a regular grid composed out of trivariate B-Splines. Please note that the utilization of B-Splines as basis functions is crucial for the explicit time step as shown in Section 4.1. The STL defines the geometrical borders to construct efficient integration rules for trimmed knot spans and additionally provides an intrinsic parametrization for contact formulations and visualization purposes. After these preprocessing steps, the required model data is passed to a solver for analysis, e.g. to LS-DYNA via a user-defined data interface.

In section 2 the underlying IGA discretization as well as the utilized solid element formulation are discussed and derived. All required embedding operations for a CAD-integrated analysis involving 3D solid models are described in Section 3. Within an explicit dynamic setting, in Section 4, the influence of trimmed knot spans on the critical time-step and the numerical stability is analyzed. To demonstrate the effectiveness of the present methodology, first numerical examples are conducted within Kratos Multiphysics [3] and LS-DYNA in section 5. Herein, a trimmed B-Spline solid cube under impact is investigated, and eigenvalue as well as explicit dynamic analyses of a BMW solid foam component are performed. The results are compared against standard FEM. We conclude with a summary and discuss possible next steps in section 6.

2 Trivariate IGA Discretization and Solid Element Formulation

The present solid IGA formulation relies on a trivariate B-Spline discretization. To this end, a parametric space $\theta = [\theta^1, \theta^2, \theta^3]$ is spanned over a three-dimensional domain Ω . Based on the knot vectors $\theta^i =$

$[\theta_1^i, \theta_2^i, \dots, \theta_{n+p+1}^i]$, the B-Spline basis functions N^i in direction θ^i are recursively constructed with the following well-known equations starting with the constant terms (polynomial degree $p = 0$):

$$N_{j,0}^i(\theta^i) = \begin{cases} 1 & \text{if } \theta_j^i \leq \theta^i < \theta_{j+1}^i, \\ 0 & \text{otherwise.} \end{cases} \quad (1)$$

For $p > 0$:

$$N_{j,p}^i(\theta^i) = \frac{\theta^i - \theta_j^i}{\theta_{j+p}^i - \theta_j^i} N_{j,p-1}^i(\theta^i) + \frac{\theta_{j+p+1}^i - \theta^i}{\theta_{j+p+1}^i - \theta_{j+1}^i} N_{j+1,p-1}^i(\theta^i). \quad (2)$$

A tensor product combines N^1, N^2 and N^3 and yields the respective function space in three dimensions. Consequently, the trivariate B-Spline solid is defined as,

$$V(\theta) = \sum_{j=1}^n \sum_{k=1}^m \sum_{l=1}^h N_{j,p}^1(\theta^1) N_{k,p}^2(\theta^2) N_{l,p}^3(\theta^3) P_{j,k,l}, \quad (3)$$

with $P_{j,k,l}$ denoting the control points. Given the bilinear form $a(u, v)$ the weak formulation including the virtual work emanating from inertia forces, damping forces, internal stresses, and external forces reads:

$$\int_{\Omega} \rho \ddot{u} \cdot v \, d\Omega + \int_{\Omega} \dot{u} \cdot \kappa \cdot v \, d\Omega + \int_{\Omega} \nabla u : C : \nabla v \, d\Omega = \int_{\Gamma} \hat{t} \cdot v \, d\Gamma, \quad (4)$$

with ρ, κ, C, \hat{t} being the density, the matrix of viscous damping coefficients, the elasticity tensor, and the traction forces, which act on the solid's boundary Γ . Following the Bubnov-Galerkin approach, the displacement field u and the test function v are discretized with the same basis functions [4].

$$u = \sum_{j=1}^n \sum_{k=1}^m \sum_{l=1}^h N_{j,p}^1(\theta^1) N_{k,p}^2(\theta^2) N_{l,p}^3(\theta^3) \hat{u} \quad (5)$$

Equivalent to classical FEM, the same paradigm holds for the discretization of the acceleration \ddot{u} and velocity \dot{u} . Considering an univariate B-Spline domain with polynomial degree p , each knot span is influenced by $n_{cp} = p + 1$ control points. In the scope of IGA, a knot span is classically considered as the equivalent to an element in standard FEM. Thus, the local element stiffness matrix of the IGA solid is assembled via the contributions of $\prod_{i=1}^3 (p^i + 1)$ active basis functions within a three-dimensional knot span.

3 Embedding Process of 3D CAD Model

Due to the nature of B-Spline bases, the continuous discretization field, as described in section 2, is restricted to simple topologies and is hence not capable of capturing arbitrarily complex shapes. To circumvent this limitation, the surface boundary of the solid CAD model is embedded into a regular B-Spline grid, which releases the requirement of complex meshing strategies. Consequently, providing

- two points A and B,
- the polynomial degree in all space directions
- and the knot span / element size in all space directions,

standard k-refinement, which incorporates order elevation and subsequent knot insertions, can be employed to generate the desired B-Spline solid. Reference [5] provides a detailed description of the respective refinement algorithms. It shall be noted that this process can be fully automated and does not require any manual operations. Fig. 1 (left) illustrates an exemplary trivariate B-Spline domain over a bounding box from point A to point B with uniform knot vectors.

As the IGA solid does not obey the geometrical model boundaries, only a portion of all knot spans will be fully contained within the physical domain, see Fig. 1 (right). Exterior and trimmed knots spans arise inevitably, which is a common obstacle for immersed boundary methods, such as the Finite Cell Method [6] to name one prominent example. Therefore, each knot span must be categorized and treated according to its location relative to the geometry boundary. To ease the CAD integration process, the B-Rep model is tessellated and embedded via lower order entities. This does not only enable the use of well-established geometrical algorithms for polygonal meshes [7], but also provides a parametrization for the imposition of Dirichlet and Neumann boundary conditions as well as for the definition of contact formulations. Due to the non-boundary-fitted IGA discretization, Dirichlet conditions are enforced in a

weak sense, whereby the Penalty method, Lagrange multiplier and Nitsche's method are possible candidates.

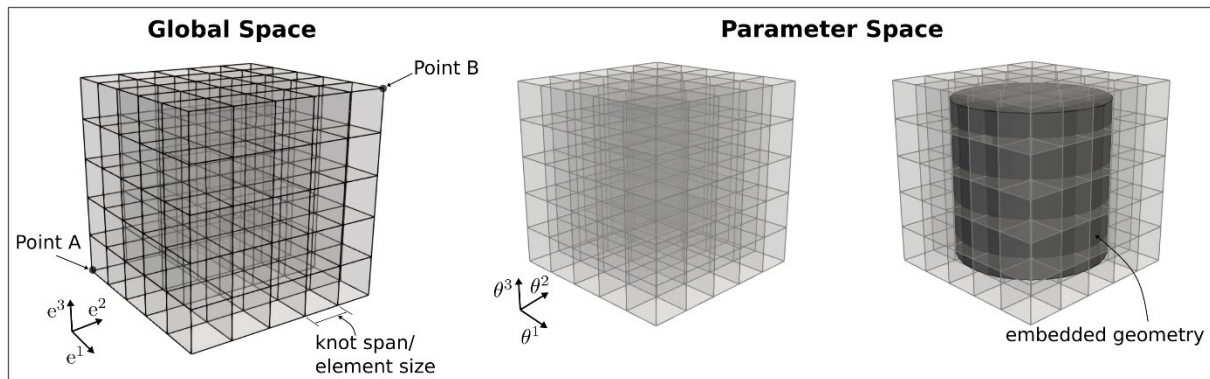


Fig.1: *B-Spline solid discretization: Global space, parameter space and parameter space with embedded geometry.*

The tessellated geometry can directly be obtained from the CAD software but could also be constructed during a preprocessing step within the FE solver. One prominent data structure is the standard tessellation/triangle language (STL), which is supported by most CAD programs and widely used in the scope of rapid prototyping and 3D-printing. The quality of the STL representation is commonly determined by various tessellation parameters, such as the minimum edge length and aspect ratio of each triangle. However, the STL representation is not used for the discretization of the field variables, but solely serves as a delimiter of the actual geometry. Thus, a moderate aspect ratio does not necessarily need to be enforced and the main objective regarding the STL mesh breaks down to an accurate geometrical representation. To this end, the desired mesh quality is solely determined by the chordal tolerance, which prescribes the maximum distance between edges on the STL and the B-Rep surface. This entails a coarse discretization at rather plane sections of the tessellated geometry, but small elements at corners, edges or heavily curved segments, which guarantees an efficient boundary representation. Moreover, due to the decoupling of FE discretization and the geometry description, an excessively fine STL mesh may affect the efficiency of the embedding operations in the preprocessing step but will not influence the computational effort during analysis. Following the B-Rep paradigm, each triangle contained within the boundary mesh (STL) is mapped and stored inside the parameter space of the B-Spline solid. As the function space is restricted to a regular grid, the mapping from physical to parametric space is achieved via simple operations such as scaling, shifting and rotating. The categorization of interior, exterior and trimmed knot spans is split into two steps. Firstly, an intersection algorithm for polygonal meshes [8] is employed to detect trimmed knot spans. To distinguish between interior and exterior ones, the center of each non-trimmed knot span is tested against the geometry boundary. Based on the normal vector of the boundary triangles in its vicinity, the center point and accordingly the entire knot span is categorized as either inside or outside. Kudela et al. established a similar inside/-outside test based on oriented point clouds in the scope of the Finite Cell Method [9].

Due to the existence of knot spans/elements with different intersection states, individual numerical integrations rules must be constructed to evaluate the terms in equation (4). As exterior knot spans are physically irrelevant, they are neglected during the computation of the system matrices. Knot spans that are fully contained within the physical domain may be evaluated by standard Gauss quadrature. However, Hughes et al. [10] show that this classical approach is not optimal regarding the number of integration points and propose the so-called half-point rule, which incorporates continuity properties across multiple knot spans. Depending on the polynomial degree of the B-Spline bases, the number of required integration points in comparison to standard Gauss quadrature can be reduced significantly (for $p = 2$ up to 70.4%, for $p = 3$ up to 75.6% and for $p = 4$ up to 78.4%) while preserving the same accuracy. For a more detailed discussion on the underlying theory and the application of the half-point rule the reader is referred to [10]. The probably most complex task arising in any immersed boundary method is the integration of trimmed knot spans, as a generic mathematical theorem for trimmed integration domains is still lacking. To this end, the moment fitting equation is solved to realize efficient integration rules even in the case of arbitrarily complex domains. We apply the adaptive point distribution scheme [11] to linearize the moment fitting equation but select only points which are located inside the physical domain. The required constant terms are evaluated by employing the divergence theorem in a similar fashion as in [12]. Thereby, the volume integral is transferred to multiple surface integrals which

are evaluated over the lower order entities of the embedded geometry. To reduce the number of integration points to a minimum an iterative point elimination algorithm [13] is utilized, whereby a non-negative Least-Square-Solver ensures positive defined weights. In contrast to classical boundary-fitted IGA, the geometry is here not delimited by the B-Spline function space. Thus, the geometrical information is solely represented via the locations and weights of the computed integration points and the active basis functions within each knot span. For simple simulation settings like an eigenvalue analysis, the data transfer between preprocessor and FE solver may therefore be limited to the B-Spline discretization field (knot vectors, polynomial degrees and control points) and a list of integration points. The geometric boundary (here STL representation) is only required for the application of boundary conditions, for contact analysis or visualization purposes within the postprocessor.

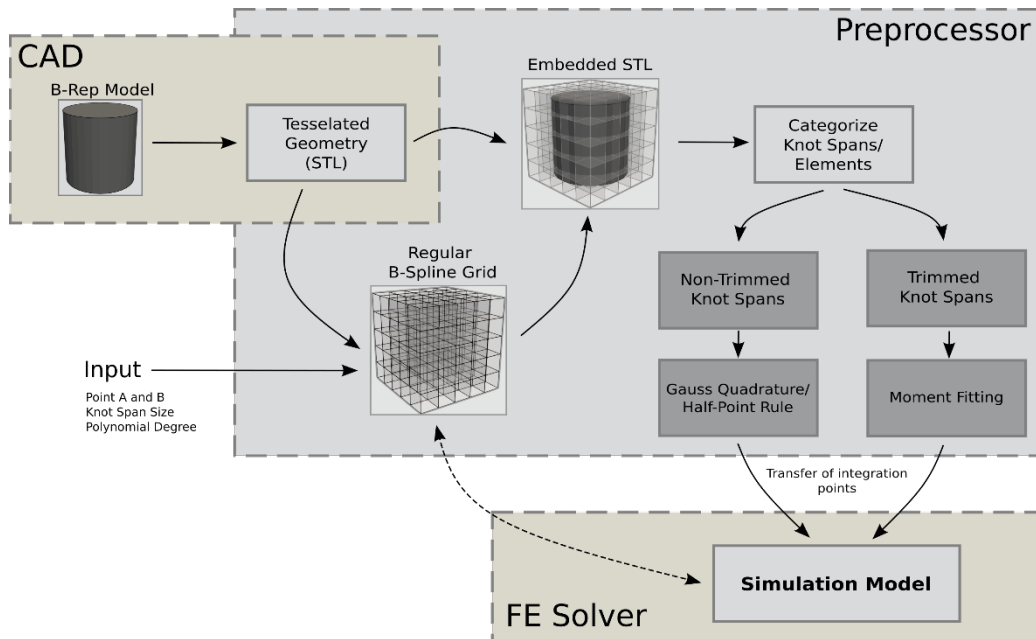


Fig.2: Workflow from CAD geometry to simulation model.

It is worth noting that all operations discussed in this section are preprocessing steps and must only be done once at the beginning of an analysis. Therefore, their computational effort is amortized when simulations with multiple iterations are conducted. Moreover, the determined integration points may even be stored and reused for different analysis settings of the same geometric model. Fig. 2 summarizes the overall workflow from CAD geometry to simulation model and shows the clear separation between the automatic preprocessing operations and the actual analysis in the FE solver. The data transfer to LS-DYNA is achieved via a user-defined interface.

4 Influence of Trimming Operations on Explicit Simulations

In this section the influence of trimmed knot spans/elements on the critical time step and the numerical stability of explicit simulations shall be discussed.

4.1 Influence of Trimmed Element Size on Maximum Eigenfrequency and Critical Time Step

Given a C^0 continuous discretization field, as encountered in standard FEM, the critical time step for explicit dynamics is approximated by the characteristic length of the smallest element - the smaller the element, the smaller the time step. As shown by Leidinger [14], this relation also holds for the size of trimmed elements in case of C^0 inter-element continuity. Therefore, arbitrarily small trimmed elements, which cannot be avoided in practice, lead to excessively small time steps and thus to infeasible simulation times. This is a major issue for most immersed boundary methods. However, in contrary to classical discretization techniques, IGA allows for higher continuities, which result in basis functions spanning across multiple knot spans. In the scope of shell element-based IGA, Leidinger [14] found that the critical time step benefits from those higher continuities, i.e. that the critical time step is practically independent of the trimmed element size for IGA. Only this characteristic makes immersed boundary methods practically feasible for explicit dynamics.

To show that the same favorable behavior is also observed for the trimmed IGA solid approach, a trimmed cube is analyzed in the following. To this end, we construct a trivariate B-Spline solid with

maximum C^{p-1} continuity, an edge length of 120mm and uniform knot vectors containing 12 knot spans/elements in each space direction. The resulting B-Spline solid cube is symmetrically trimmed from each side by the trimming distance $\hat{\theta}$, as depicted in Fig. 3. To analyze the influence of the trimming operations on the critical time step, the following eigenvalue problem is solved for different values of $\hat{\theta}$:

$$(K + \omega^2 M)\phi = 0,$$

with K, M, ω, ϕ denoting the stiffness matrix, the lumped mass matrix, the angular eigenfrequency and their corresponding eigenmodes.

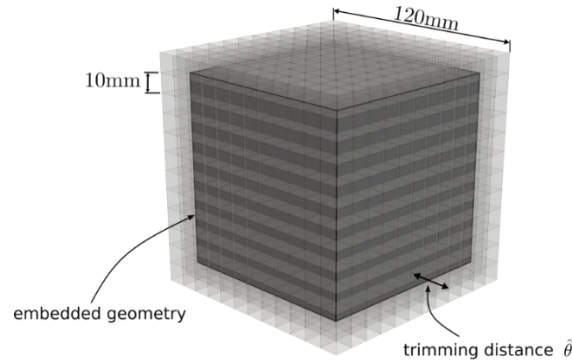


Fig.3: Trimmed cube: Cube embedded into a B-Spline solid discretization with indicated element size and trimming distance $\hat{\theta}$.

The utilized linear elastic material parameters are listed in Table 1. Fig 4 shows the computed maximum angular eigenfrequencies ω_{max} over the trimming distance $\hat{\theta}$ for different polynomial degrees p of the underlying B-Spline bases. In all cases C^{p-1} continuity is employed. The dotted line shall provide a reference value obtained from a structured FEM mesh with linear basis functions and a constant element edge length of 10mm.

Young's modulus E	Poisson ratio ν	Density ρ
210 000 N/mm ²	0.33	7.8e - 6 kg/mm ²

Table 1: Trimmed cube: Material properties

Due to the resulting C^0 discretization for $p = 1$ (blue curve), the angular eigenfrequency is close to the reference value if only small portions of the knot spans are trimmed. However, when the trimming distance approaches the knot span length ($\hat{\theta} = 10, 20, 30, \dots$), small elements occur and the angular eigenfrequency tends to infinity. Consequently, the critical time step

$$\Delta t_{crit} = 2/\omega_{max}$$

drops to infeasible values. Similar results must be expected for any discretization technique, which involves trimming operations and exhibits C^0 continuity across element boundaries. However, the present B-Spline bases allow to elevate the continuity by increasing the polynomial degree. In fact, for any polynomial degree $p > 1$ the maximum angular eigenfrequency is bounded to practically feasible values if $\hat{\theta} > 10 = 1 * \text{element length}$. Moreover, the eigenfrequencies become smaller with increasing polynomial degree and independent of the trimmed element size. Nevertheless, the boundary knot spans ($\hat{\theta} < 10$) exhibit a contrary behavior. This effect stems from the shape of the basis functions and the distribution of their associated control points. Considering an open knot vector, C^0 continuity is enforced at either end of the patch. Thus, the control point density is increased and the basis functions become steeper as their local support is reduced. This leads to higher stiffness and lower mass entries and hence to larger eigenfrequencies. For a more detailed discussion on the effect of boundary knot spans the reader is referred to [14]. To prevent that the critical time step suffers from this effect, the B-Spline discretization domain is chosen large enough, such that all boundary knot spans are outside the physical domain. Consequently, all boundary knot spans are naturally considered as trimmed off during the embedding process. Following this approach, the critical time step of the trimmed B-Spline solid can be increased beyond the FE reference value. In conclusion, the results obtained for IGA shells [14] could be successively reproduced for solids. Therewith, it is exemplarily demonstrated that trimmed B-Spline solids are suitable for explicit dynamics as they allow a practically feasible critical time step.

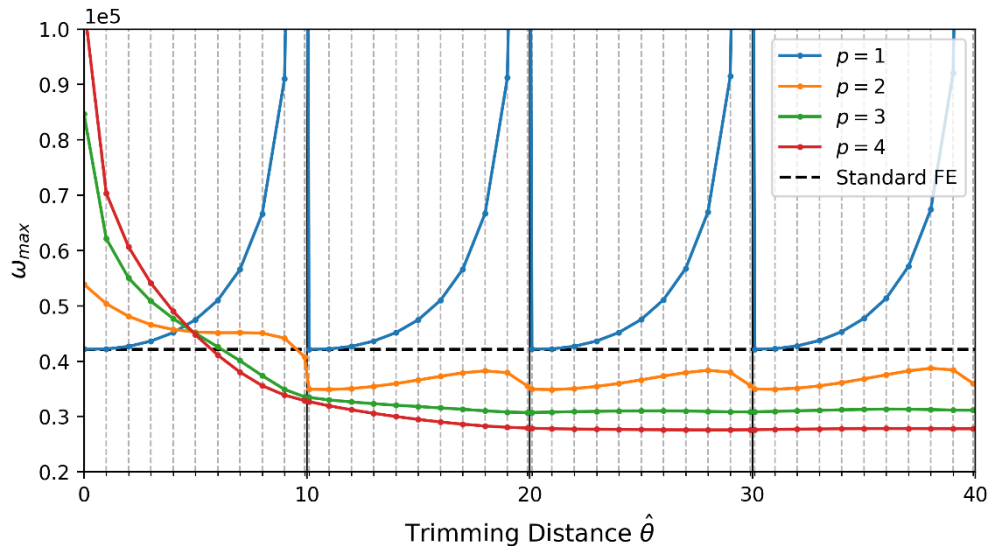


Fig.4: *Trimmed cube: Maximal angular eigenfrequency ω_{max} over the trimming distance $\hat{\theta}$ for different polynomial degrees.*

4.2 Numerical Instability through Light Control Points

As mentioned in the previous subsection, small trimmed elements appear regularly for complex industrial models. Such small trimmed elements implicate basis functions with small support in the material domain and consequently control points with low mass and stiffness. Because of their small mass, these control points are commonly denoted as light control points. As already reported for shells [14], light control points may exhibit extremely high displacements and velocities, which in turn may lead to premature solver terminations due to out-of-range values, especially in highly dynamic simulations. To prevent light control points from having extremely large values, Leidinger [14] proposed an effective stabilization technique for trimmed shells. A similar approach is currently implemented and successfully used in LS-DYNA. Such a stabilization technique may also be implemented for trimmed solids in the future. However, currently no stabilization is available for trimmed solids and therefore the examples in the following section are particularly designed such that small trimmed elements are avoided.

5 Examples

To show the effectiveness of the presented trimmed B-Spline solid approach within the field of explicit dynamics, first crash-type simulations, namely a cube with an impacting sphere and a BMW vehicle component pinched between plates, are performed in LS-DYNA and compared to standard finite element analysis (FEA).

5.1 Trimmed Cube with Impacting Sphere

A trimmed solid B-Spline cube with an impacting rigid FE sphere, see Fig. 5, shall demonstrate the capability of the trimmed B-Spline solid approach regarding highly dynamic nonlinear problems including large deformations and contact in LS-DYNA. It shall furthermore provide a comparison to standard FEA in terms of accuracy and numerical effort.

The rather simple cube geometry allows to preclude the existence of small trimmed elements, which would require an additional stabilization method as described in Section 4.2. The cube with an edge length of $a = 100\text{mm}$ is modelled as a foam with `*MAT_CRUSHABLE_FOAM` and discretized with an element length of 4mm and 16mm for both standard solid FEA (ELFORM=10, 1-point tetrahedron) and trimmed solid IGA (quadratic elements), see Fig.5b. Please note that for the IGA cubes in Fig. 5b, the regular yellow mesh indicates the active elements (interior and trimmed elements) of the B-Spline solid discretization, the black dots represent the corresponding active control points and the green tetrahedron mesh shows the actual cube geometry embedded into the yellow B-Spline solid grid. For the latter, a fine 4mm element length is applied for both IGA configurations since it is only used to model contact and for visualization purposes. Neither are these elements evaluated nor do they affect the critical time step. This is a great advantage of the presented approach, as the geometry description can be completely decoupled from the actual IGA discretization field. The impacting sphere with a diameter of $d = 70\text{mm}$ and the underlying plate are discretized with standard finite elements and considered as rigid. A segment-based penalty contact (`*CONTACT_SURFACE_TO_SURFACE` with `SOFT=2`) including friction is used.

Cross-section cuts of the deformed shapes right after the impact are depicted in Fig.6. For both FEA models, the linear discretization with C^0 inter-element continuity can be observed along the indentations, whereby the results for the 4mm model reveal a qualitatively better deformation pattern. For IGA on the other hand, the shape of the indentation is smooth, even for the coarse 16mm B-Spline discretization. The resulting contact force between the sphere and the cube over time is given in Fig.7. Thereby, the results of the 4mm and 16mm IGA model agree well with the results of the 4mm FEA model, which is here considered as reference solution. By comparing the 4mm and the 16mm FEA results, the discrepancy between fine and coarse discretization is clearly visible, whereas IGA provides reasonable values in either case. Hence, for this particular example a much coarser discretization and therefore a much lower number of DOFs can be used with the trimmed B-Spline solid approach.

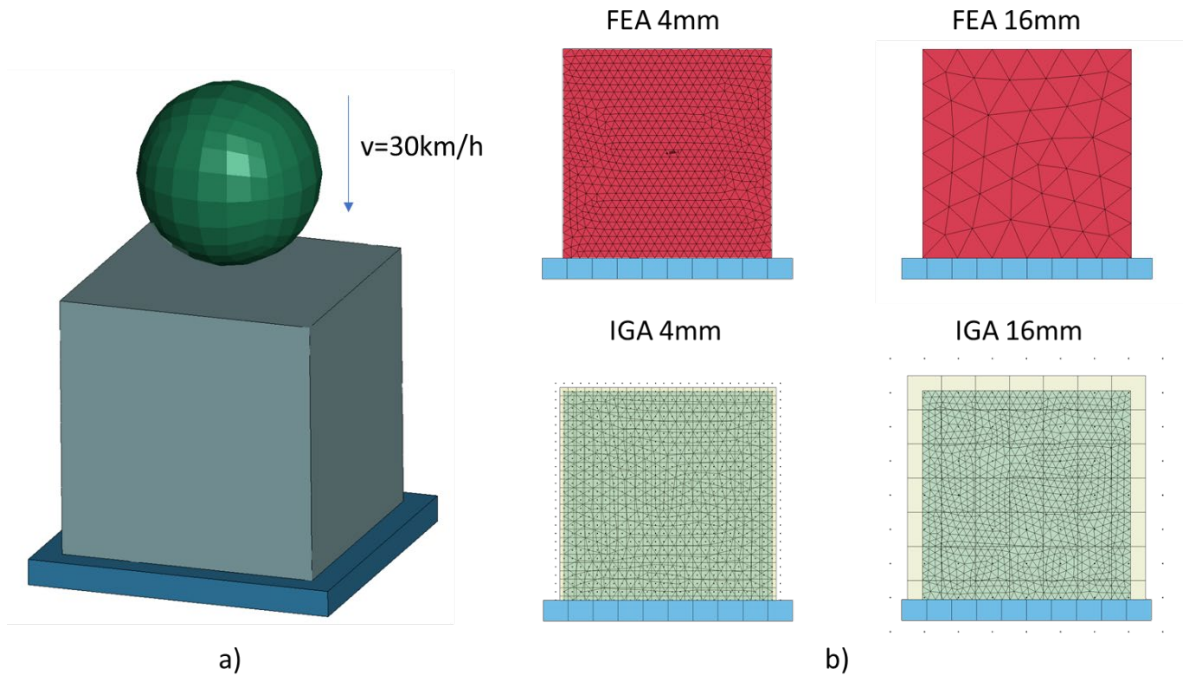


Fig.5: *Trimmed cube with impacting sphere: Problem description in a) and different discretizations for FEA and IGA in b).*

The number of integration points as well as the average CPU time for the different simulation scenarios are provided in Table 2. Regarding the integration points, it is shown that the trimmed solid IGA approach requires slightly more integration points than standard FEA for the same element size. This comparison is affected by the ratio between trimmed and untrimmed elements, since trimmed elements usually have more integration points than untrimmed ones. For this particular example, the isogeometric simulations take approximately twice as long as the standard finite element simulations for the same element size and the same initial time step size. However, due to the higher ansatz order and continuity within the B-Spline domain, the 16mm IGA mesh is sufficient to reproduce the 4mm FEA results, as shown in Fig.7. If these two scenarios are compared, trimmed IGA is a competitive candidate regarding computational cost and simulation time. Moreover, the potential of a larger time step as shown in Fig.4 has not been exploited. It is also worth noting that the implementation of the trimmed B-Spline solids is not yet optimized for efficiency. Therefore, the listed simulation times shall only be considered as an approximate indication about the efficiency of the compared methods.

To conclude, the present observations suggest that trimmed solid IGA yields similar or better results, while also being cost-competitive compared to standard solid FEA.

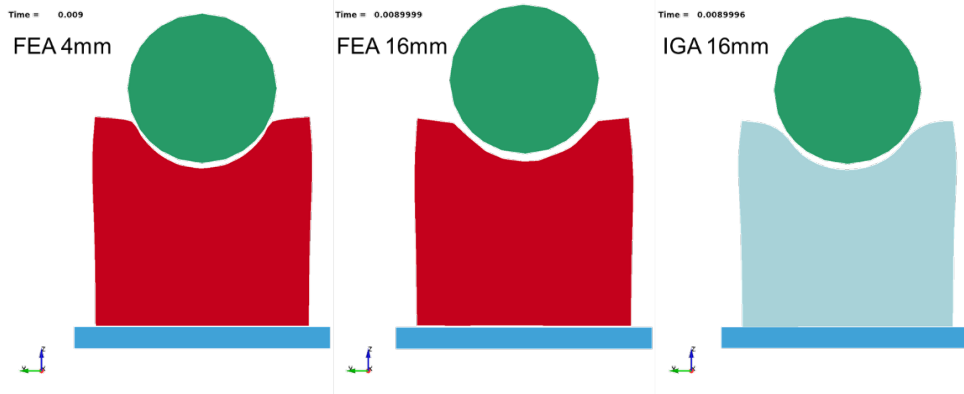


Fig.6: Trimmed cube with impacting sphere: Cross-section cuts of deformed shapes after impact.

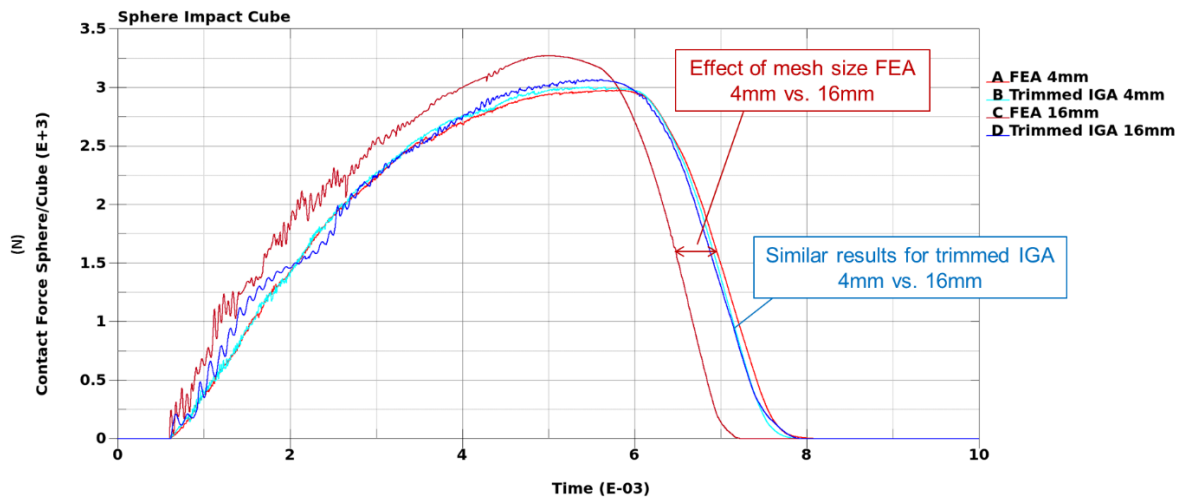


Fig.7: Trimmed cube with impacting sphere: Contact force between sphere and cube over time for different FEA and IGA models.

Model	# Integration Points	CPU time average in s (8 CPUs)
FEA 4mm	71 808	695
Trimmed IGA 4mm	84 585	1308
FEA 16mm	1 529	297
Trimmed IGA 16mm	3 463	687

Table 2: Trimmed cube with impacting sphere: Number of integration points and average CPU time.

5.2 Analyses of a BMW Foam Component

This example shall demonstrate the capability of the trimmed B-Spline solid approach to capture and simulate complex industrial models, namely an energy-absorbing BMW foam component. First, an eigenvalue analysis of a fine discretization is performed with Kratos Multiphysics [3] and compared to standard FEA in terms of accuracy and numerical effort. After that, the foam component is pinched between two FE plates and studied through an explicit dynamic simulation in LS-DYNA including large deformations and (self-)contact. For this scenario a relatively coarse discretization is used in order to avoid the appearance of small trimmed elements, see Section 4.2. In both cases, the trimmed IGA solid model was automatically generated from a STEP file as described in Section 3. The geometry of the BMW foam component is embedded into a B-Spline discretization field with $35 \times 19 \times 30$ quadratic elements, whereof only 5599 elements are active (interior or trimmed), as shown in Fig.8. Fig. 9 depicts the reference FE model with 57093 1-point tetrahedral elements. A linear elastic material model is utilized throughout all eigenvalue analyses.

The first and the second eigenmodes for both the trimmed B-Spline solid model as well as the standard FE model are depicted in Fig.10 and Fig.11 respectively. Despite the coarser IGA discretization, a qualitatively good agreement between IGA and standard FE is observed. Fig.12 provides a convergence study for the first four eigenvalues and a varying B-Spline solid discretization. Thereby, the dashed lines represent the reference values retrieved from the standard FE model and 57093 1-point tetrahedral

elements. In comparison to the FE model, the trimmed B-Spline solid yields similar results already with a much lower number of integration points, e.g. with the configuration exhibiting an approximate element size of 10mm and 26962 integration points, which shows the superior analysis properties and efficiency of the proposed trimmed B-Spline solid approach.

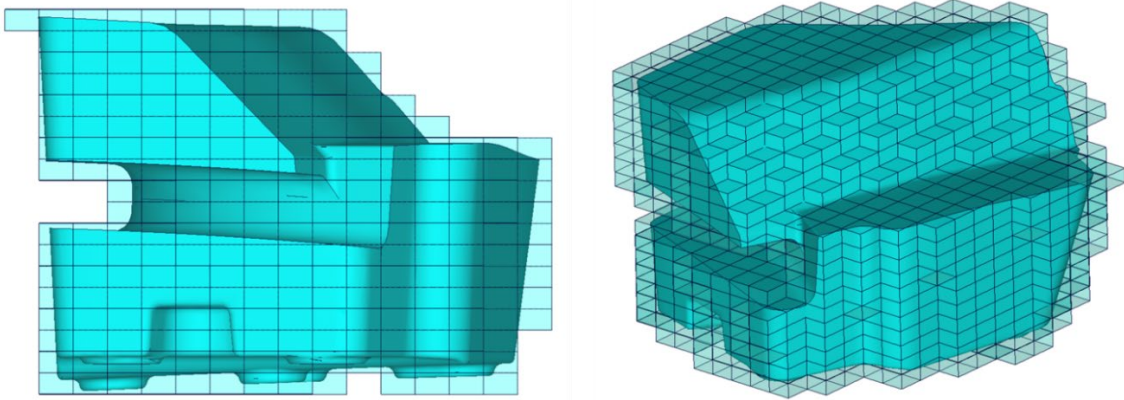


Fig.8: *BMW foam component: Model geometry embedded into a fine B-Spline solid discretization.*

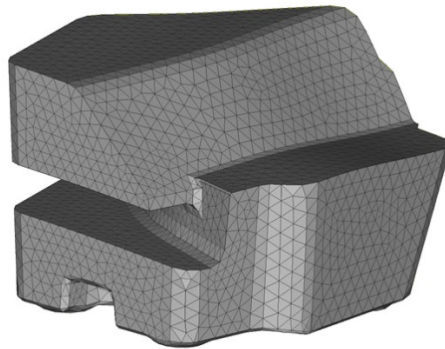


Fig.9: *BMW foam component: Standard finite element model used as a reference.*

Finally, the foam component is studied in a realistic explicit dynamic simulation scenario with large deformations and (self-)contact. This example with a relatively coarse discretization of $7 \times 4 \times 6$ elements (90 active elements) as shown in Fig.13 is not intended to provide highly accurate results, but rather to demonstrate the general ability to analyze complex models in crash-type scenarios.

The foam component pinched between two solid FE plates (bottom plate fixed, top plate with a prescribed displacement of 2m/s) is shown in Fig.14. A segment-based penalty contact (`*CONTACT_AUTOMATIC_SINGLE_SURFACE` with `SOFT=2`) including friction is used. As shown in Fig.14, the trimmed B-Spline solid model is able to undergo extremely large deformations. Furthermore, contact and even self-contact is accurately captured. Fig.15 provides a comparison between the trimmed B-Spline solid model with a coarse discretization and the results of a fine FE solid model. As expected, the coarse B-Spline model shows a stiffer behavior, e.g. the discontinuity introduced by the notch cannot be captured. Nevertheless, a good qualitative agreement between the two deformed shapes can be observed.

From the eigenvalue analysis and the explicit dynamic analysis of this BMW component it can be concluded that the proposed trimmed B-Spline solid approach is generally able (i) to provide accurate results with a lower number of elements and integration points compared to standard FEA and (ii) to simulate complex industrial models in crash-type scenarios. Of course, a suitable stabilization method for light control points is still required for real industrial applications. This will be the immediate next step in the development process.

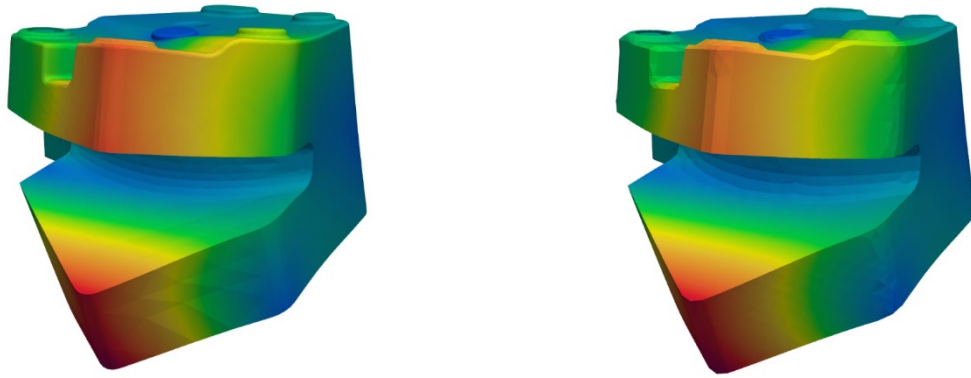


Fig.10: First eigenmode: Trimmed B-Spline solid model (left) and standard FE model (right).

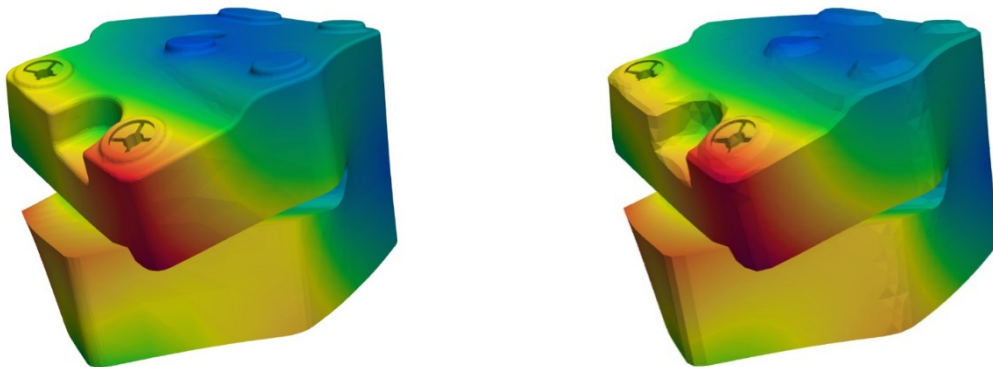


Fig.11: Second eigenmode: Trimmed B-Spline solid model (left) and standard FE model (right).

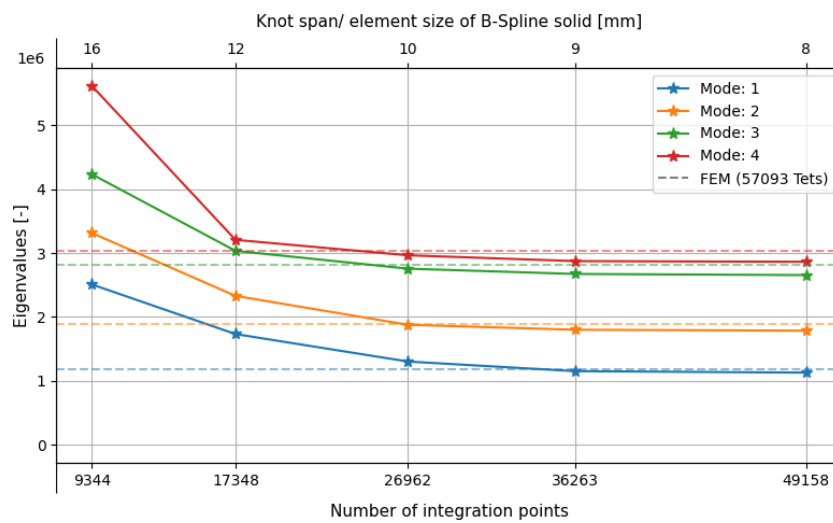


Fig.12: BMW foam component: Convergence study and comparison with standard FE solid results.

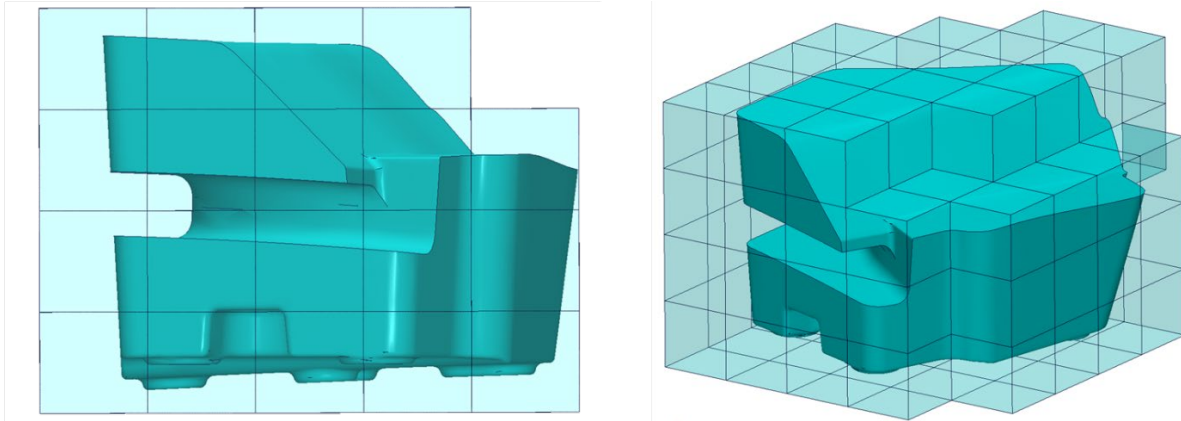


Fig.13: BMW foam component: Model geometry embedded into a coarse B-Spline solid discretization.

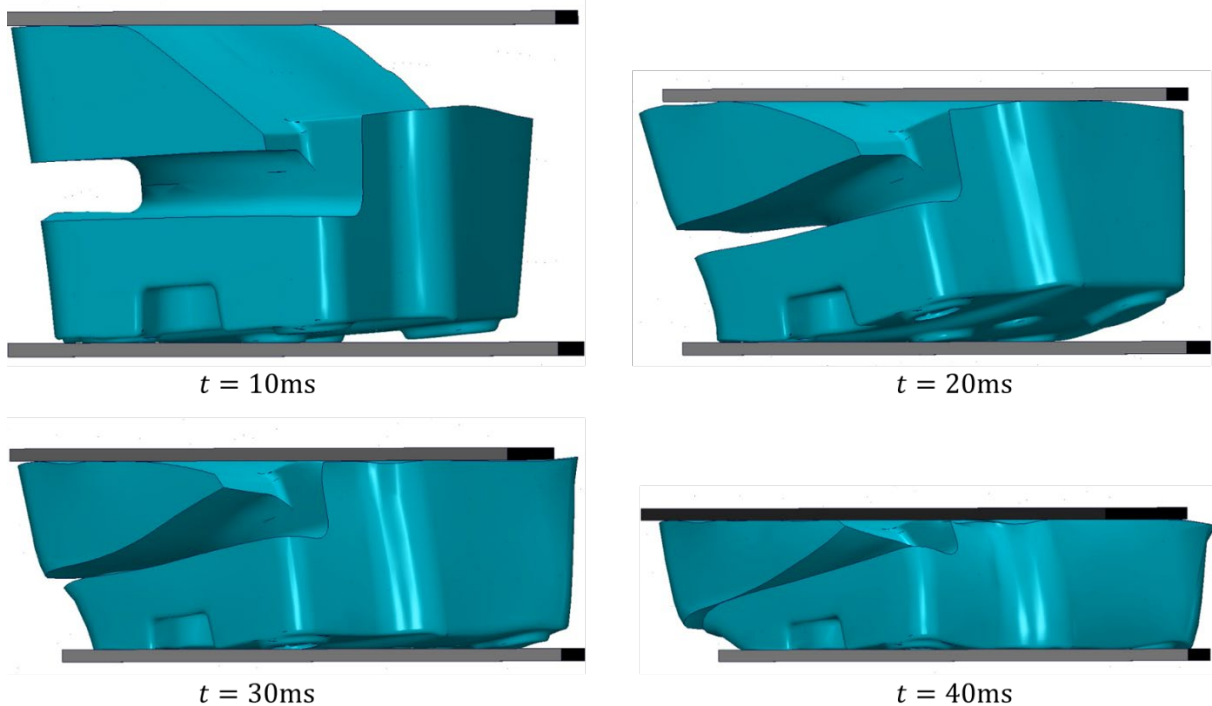


Fig.14: BMW foam component: Trimmed B-Spline solid model pinched between two solid FE plates.

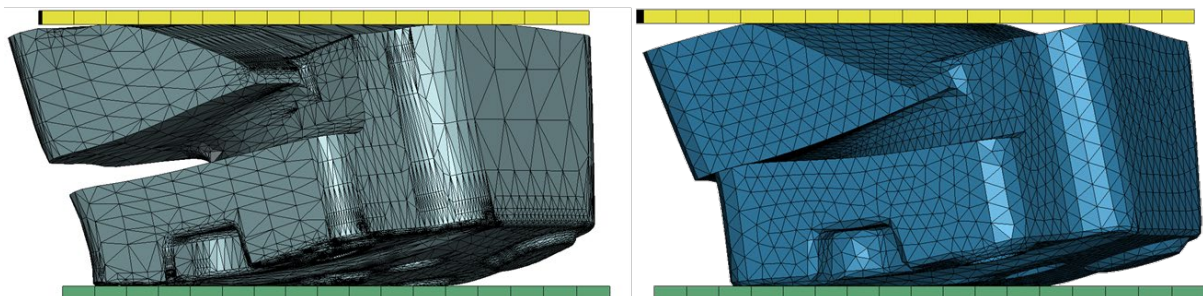


Fig.15: BMW foam component: Comparison between a trimmed B-Spline solid model visualized through the STL representation (left) and a standard FE solid model (right).

6 Conclusion and Outlook

In the present work, a CAD-integrated analysis workflow for 3D solid models with focus on explicit dynamics is presented. To fill the interior void, which is classically encountered inside solid B-Rep models, the CAD geometry is embedded into a B-Spline-based discretization field. Therewith, the requirement of boundary-fitted meshes is avoided while at the same time the discretization enables the use of standard finite element formulations. Following the classical IBRA concept, the geometrical

boundaries are stored in the parameter space of the B-Spline solid and utilized to define numerical integration domains. To enable an intrinsic parametrization for the imposition of boundary conditions the geometry is tessellated and embedded via lower-order entities. We make use of the continuity properties of the B-Spline bases to realize practically feasible values for the critical time step. Depending on the polynomial degree, it is shown that the critical time step can be increased beyond the value of standard explicit FE simulations with equivalent minimal element size. However, to exploit the full potential of the B-Spline bases, C^{p-1} continuity must be employed and the effect of the boundary knot spans must be removed. For the latter requirement, it is proposed to construct the B-Spline discretization large enough such that all boundary knot spans are located outside the physical domain and consequently are considered as trimmed knot spans during the embedding process. If those propositions are met, the obtained results suggest that standard critical time step estimations for solid elements can be adopted for trimmed trivariate B-Spline domains.

The presented method is currently limited through the existence of so-called light control points. Assuming that the influence of light control points on the solution vector is negligibly small, they may be detected and entirely removed from the system of equations. Another remedy is suggested in [14]. In a similar context, Leidingner resolves the instability issue by adding a penalty term to the excessively small stiffness entries. The effectiveness of both methods for trimmed B-Spline solids is still to be investigated. If an expedient solution is found, more complex examples shall be analyzed and compared to standard FEM regarding accuracy and numerical effort.

Due to the very promising results obtained with the proposed trimmed B-Spline solid approach, the current prototypical implementation of the user-defined data interface will be enhanced into a more efficient and firm implementation within LS-DYNA. Also the fully-automated preprocessing operations, which are currently performed in an academic software environment, will be available in a similar manner in a standard preprocessor in the near future. However, the operations related to the generation of integration points are planned to be realized within the solver.

7 Literature

- [1] Hughes T.J.R., Cottrell J.A., Bazilevs, Y.: "Isogeometric analysis: CAD, finite elements, NURBS, exact geometry and mesh refinement", *Computer Methods in Applied Mechanics and Engineering*, Vol. 194 (39-41), 2005, 4135-4195.
- [2] Breitenberger M., Apostolatos A., Philipp B., Wüchner R., Bletzinger K.-U.: "Analysis in computer aided design: Nonlinear isogeometric B-Rep analysis of shell structures", *Computer Methods in Applied Mechanics and Engineering*, Vol. 284, 2015, 401-457.
- [3] <https://github.com/KratosMultiphysics/Kratos>
- [4] Hughes T.J.R., "The Finite Element Method: Linear Static and Dynamic Finite Element Analysis", Dover Publications, Mineola, NY, 2000.
- [5] Piegl L., Tiller W., "The NURBS Book", *Monographs in Visual Communication*, Second ed. Springer-Verlag, New York, 1997.
- [6] Düster A., Parvizian J., Yang Z. and Rank E., "The finite cell method for three-dimensional problems of solid mechanics", *Computer Methods in Applied Mechanics and Engineering*. Vol. 197 (45-48), 2008, 3768– 3782.
- [7] Botsch M., Kobbelt L., Pauly M., Alliez P. and Lévy B., "Polygon mesh processing", CRC press, 2010.
- [8] Campen M., Kobbelt L., "Exact and Robust (Self-)Intersections for Polygonal Meshes", *Computer Graphics Forum*, Vol. 29, 2010, 397-406.
- [9] Kudela L., Kollmansberger S., Almac U., Rank E., "Direct structural analysis of domains defined by points clouds", *Computer Methods in Applied Mechanics and Engineering*, Vol. 358, 2020, 112581.
- [10] Hughes T.J.R., Reali A. Sangalli G., "Efficient quadrature for NURBS-based isogeometric analysis", *Computer Methods in Applied Mechanics and Engineering*, Vol. 199 (5-8), 2010, 301-313.
- [11] Hubrich S., Joulaiian M., Düster A., "Numerical integration in the finite cell method based on moment-fitting", *Proceedings of 3rd ECCOMAS Young Investigators Conference, 6th GACM Colloquium on Computational Mechanics*, Aachen. 2015.
- [12] Joulaiian M., Hubrich S., Düster A., "Numerical integration of discontinuities on arbitrary domains based on moment fitting", *Computational Mechanics*, Vol. 57, 2016, 979-999.
- [13] Nagy A., Benson D., "On the numerical integration of trimmed isogeometric elements", *Computer Methods in Applied Mechanics and Engineering*, Vol. 284, 2015, 165-185.

- [14] Leidinger L., “Explicit Isogeometric B-Rep Analysis for Nonlinear Dynamic Crash Simulations”, Dissertation, Technical University of Munich, 2020.